# ZnO Nanoparticles Applied to Bioimaging and Drug Delivery

*Huan-Ming Xiong**

**The last decade has seen significant achievements in biomedical diagnosis and therapy at the levels of cells and molecules. Nanoparticles with luminescent or magnetic properties are used as detection probes and drug carriers, both in vitro and in vivo. ZnO nanoparticles, due to their good biocompatibility and low cost, have shown promising potential in bioimaging and drug delivery. The recent exciting progress on the biomedical applications of ZnO-based nanomaterials is reviewed here, along with discussions on the advantages and limitations of these advanced materials and suggestions for improving methods.**

## 1. Introduction

Semiconductor nanoparticles, due to their unique physical and chemical properties, have significant advantages in biomedical applications, such as bioimaging and drug delivery.[1–5] The unique properties are based on their size similarity with biomolecules, their abundant functionality on large surface areas, and their quantum size effects. For example, quantum-dot-tagged polymer beads with encoded fluorescence can theoretically recognize millions of biological targets.[6] However, most semiconductor nanoparticles are toxic to animals, and their biocompability is poor in vivo.[7–9] ZnO nanoparticles, as a new type of low-cost and low-toxicity material, are expected to perform better in biomedical applications.

In a well-designed in vivo experiment, ZnO-based nanocomposites will be injected into a mouse through its tail vein and transferred to the tumor. The nanocomposites could be ZnO nanoparticles loaded with drugs or ZnO hollow spheres containing drugs, and they will be able to penetrate cancer cells through specific ligand–receptor recognition or nonspecific binding forces based on hydrophobic or Coulombic interactions. Since the tumor and cancer cells have acidic environments–especially in lysosomes and endosomes, the ZnO nanostructures will decompose and release the drugs. This process will be detectable by UV light irradiation when the tumor is close to the mouse skin or by magnetic resonance imaging (MRI) when the ZnO nanoparticles are doped with magnetic elements. The anticancer drugs, the $Zn^{2+}$ ions resulting from ZnO decomposition, and reactive oxygen species (ROS) will be able to destroy the cancer cells cooperatively. As a result, tumor growth and development will be suppressed. This experiment will likely be realized in the near future because the necessary preliminary work has already been achieved in recent reports which are outlined in the following sections.

Prof. H.-M. Xiong
Department of Chemistry
Fudan University
Shanghai, 200433, P. R. China
E-mail: hmxiong@fudan.edu.cn

**DOI: 10.1002/adma.201301732**

## 2. ZnO Nanoparticles for Bioimaging

In comparison with traditional organic fluorescent dyes, semiconductor nanocrystals possess better photoluminescent properties, including a broad absorption, a narrow and symmetric emission band, a large Stokes shifts and weak self-absorption, a tunable emission wavelength based on quantum size effects, and high stability against photo-bleaching.[10–12] However, typical quantum dots (QDs) such as CdSe and CdTe exhibit serious toxicity to biological systems,[13–15] and large-scale production would cause environmental pollution. During the past decade, many Cd-free QDs have been synthesized and tested in vitro or in vivo, e.g., ZnSe,[16] carbon,[17] and rare earth nanoparticles.[18] Among them, ZnO nanoparticles are a newer type of promising candidate because of its high safety, low price, lack of polluting effects, and good stability against air and sunlight.[19] However, the synthesis of luminescent ZnO nanoparticles with good stabilty in water is a challenge to researchers. ZnO visible fluorescence arises mainly from its surface defects, which can be destroyed by water molecules. Proper surface modification is key for resolving this problem.[20]

Sol–gel routes are regarded as the optimal method for modifying ZnO QDs because synthetic reactions near room temperature do not harm ZnO surface defects, and wet chemical techniques have been developed well.[21] Nevertheless, those previously reported ZnO nanoparticles with various capping groups, including polyvinylpyrrolidone (PVP),[22] oleic acid (OA) together with diethanolamine (DEA),[23] polyethylene glycol methyl ether (PEGME),[24] polymethylmethacrylate (PMMA),[25] and polystyrene (PS),[26] were not suitable for bioimaging. Some of them were insoluble or unstable in water, while others suffered from low luminescent efficiency or a single blue emission that could be covered by the autofluorescence of the cells.[27] In 2008, our research group invented a new route, called two-step polymerization for coating ZnO nanoparticles with a binary

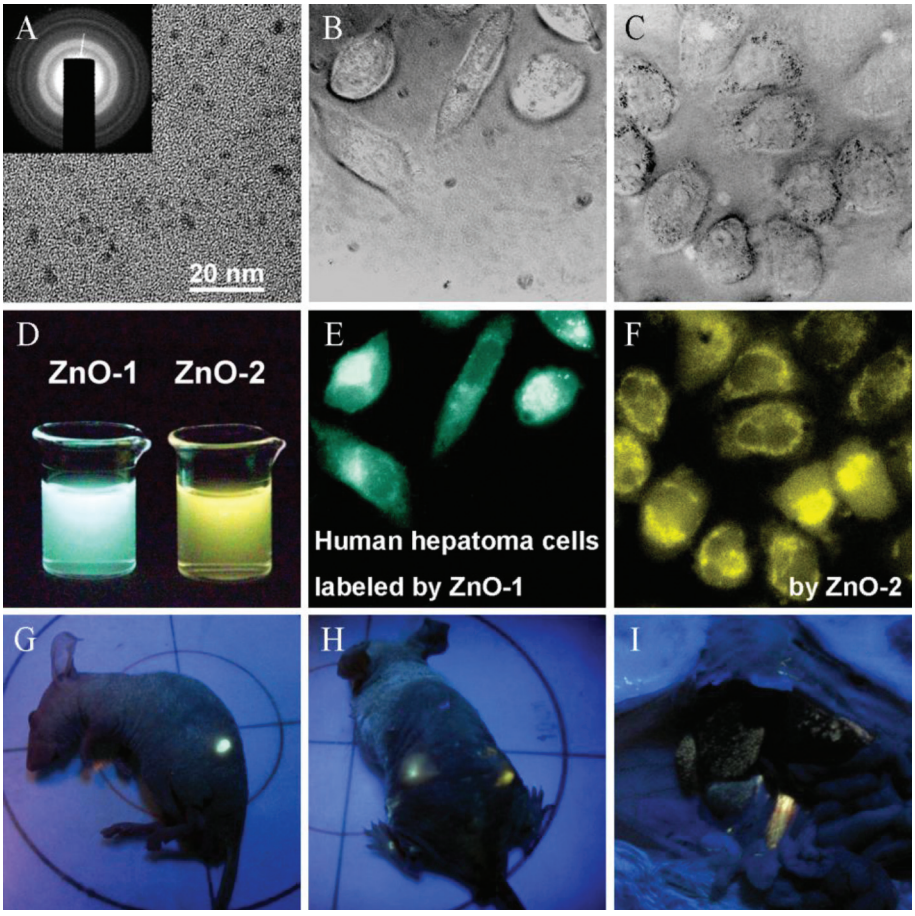


**Figure 1.** A) High-resolution transmission electron microscopy (HRTEM) image of the ZnO@polymer core–shell nanoparticles, with the inset showing the electron diffraction pattern of the same sample. B,C) Differential interference contrast (DIC) pictures of the cells after incubation with ZnO@polymer samples that were labeled as ZnO-1 (B) and ZnO-2 (C). ZnO-1 and ZnO-2 have different sizes so that their emission colors are different due to the quantum size effects. D) Photograph of the aqueous solutions of samples ZnO-1 and ZnO-2 under a UV lamp. E,F) Confocal fluorescence images of the cells, corresponding to B (E) and C (F). G,H) Mice under UV light after intradermal injection of sample ZnO-1 (green) and ZnO-2 (yellow). I) A sacrificed mouse under UV light after intravenous injection of sample ZnO-2. Reproduced with permission.[28,29] Copyright 2008 American Chemical Society (A–F).

polymer shell that contains an internal layer of hydrophobic polyester and an external layer of hydrophilic polyether.[28] Such ZnO@polymer core–shell nanoparticles exhibited very stable luminescence in aqueous solutions (quantum yield over 50% for weeks), and they were applied to cell imaging successfully for the first time (**Figure 1**). The nanoparticles could also be injected into mice, and they did not show any significant toxic effects in clinical urine and blood analyses as well as in routine histopathological analyses,[29] but their luminescence was not stable in animal blood. Later, ZnO QDs coated with a silica shell and silane groups were developed extensively;[30–34] they showed better stability in cell culture and animal blood. Despite these advances, the synthesis of luminescent ZnO QDs with stable performance in vivo remains a challenge to scientists.

Since the ZnO bandgap (3.37 eV at room temperature) is located in the UV region, UV light is necessary to excite ZnO fluorescence.[35,36] However, UV light is not suitable for most in vivo experiments because it can only penetrate the skin by several millimeters. Doping ZnO nanoparticles with magnetic elements was suggested to obtain new binary probes with both fluorescent and magnetic functions, so that the labeled tissues deep within the animal body could be detected by MRI techniques. However, many ZnO nanoparticles doped with conventional magnetic elements, such as Fe, Co, Ni, and Mn, showed almost no luminescence in the visible region.[37–42] One reason is that doping nanocrystals usually requires high temperature treatment, but under such conditions the defect concentration in ZnO nanoparticles will decrease and the defect-related visible emission will be weakened. The other explanation is that the unoccupied orbitals of transition metal ions can trap the photo-generated electrons of the nanoparticles so as to quench ZnO fluorescence. In contrast, ZnO nanoparticles doped with main group[43,44] and rare earth[45,46] elements were reported to possess significantly enhanced luminescence. For example, $Gd^{3+}$-doped ZnO nanoparticles were prepared in a sol–gel route and employed to label human cervical-cancer HeLa cells, which could be detected by both MRI and fluorescence microscopy.[47] MRI exhibits lower sensitivity and resolution than fluorescent

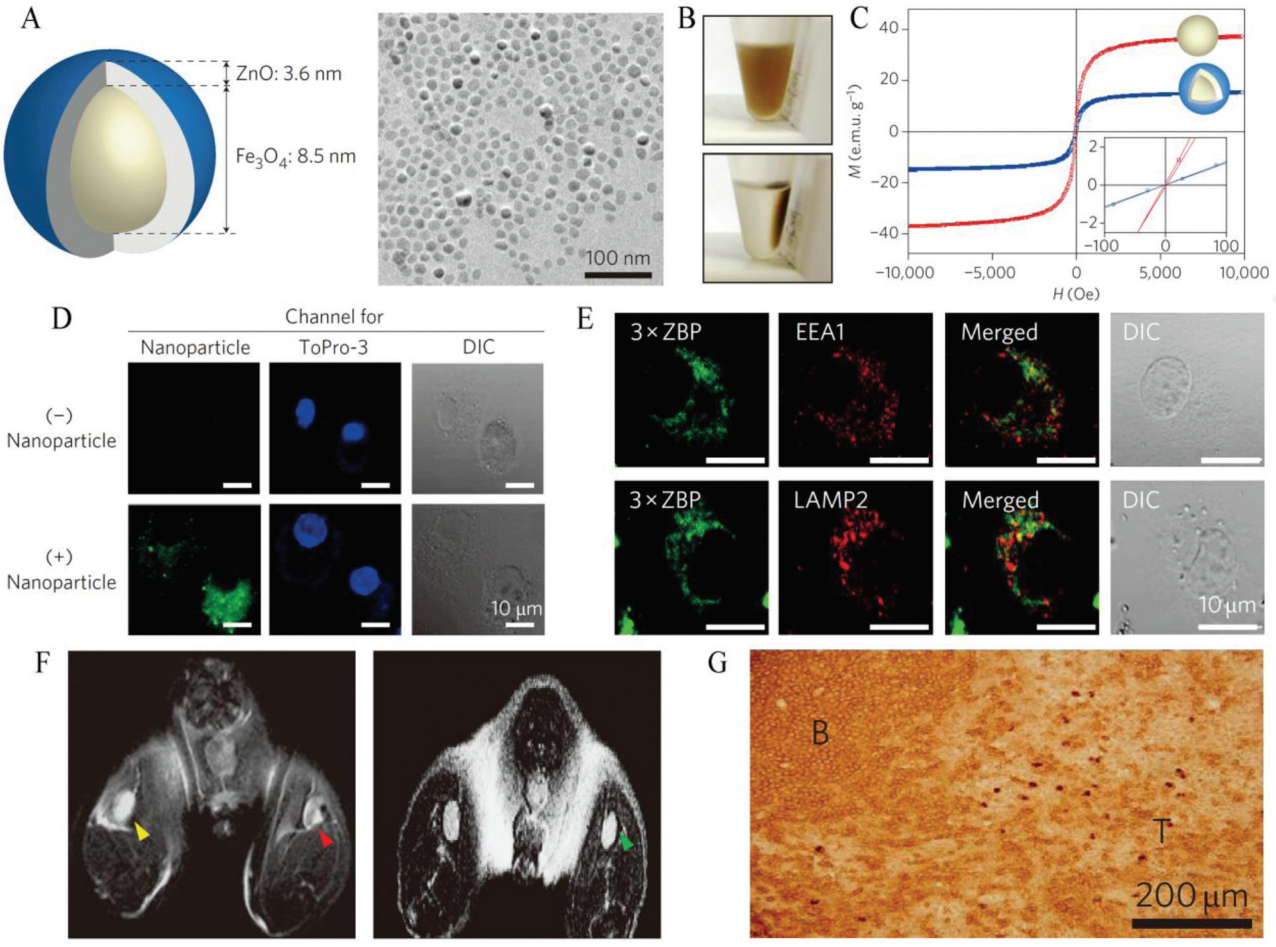


**Figure 2.** A) Structural scheme (left) and TEM image (right) of the $Fe_3O_4$@ZnO core–shell nanoparticles. B) Photographs showing the homogeneous dispersion of nanoparticles (brown) in phosphate-buffered saline (top) and clear transparent solution after the nanoparticles gather due to the application of an external magnet (bottom). C) Magnetic hysteresis curves of the $Fe_3O_4$ core (red) and the $Fe_3O_4$@ZnO nanoparticles (blue). Inset: details of the hysteresis curves around zero field. D) Fluorescence images of DCs loaded without (top) or with (bottom) nanoparticles (green). Nuclei (blue) were stained with ToPro-3. E) Fluorescence images of DCs incubated with $Fe_3O_4$@ZnO–3×ZBP complexes. Intracellular 3×ZBP (green) is revealed along with the endosomes and lysosomes, which were stained using EEA1 and LAMP2, respectively. F) In vivo MRI images of draining lymph nodes of a mouse (left) injected with DCs labeled with $Fe_3O_4$@ZnO (red arrow) or ZnO nanoparticles (yellow arrow) into the ipsilateral footpads. The right image shows a draining lymph node (green arrow) of a mouse injected with $Fe_3O_4$@ZnO nanoparticles alone—without DCs. G) Representative immunohistochemistry of the draining lymph node after injection with $Fe_3O_4$@ZnO-nanoparticle-labeled DCs (dark brown dots). T: T-cell zone (Thy1.2$^+$); B: B-cell follicle (B220$^+$). Reproduced with permission.[48] Copyright 2011 Nature Publishing Group.

imaging, but it penetrates deeply into animal tissues and thus compensates the limitations of in vivo optical imaging.

Recently, Kim and Seong and co-workers[48] synthesized $Fe_3O_4$@ZnO core–shell nanoparticles to deliver carcinoembryonic antigen (CEA) into dendritic cells (DCs) to realize mouse cancer immunotherapy. These $Fe_3O_4$@ZnO core–shell nanoparticles not only acted as nanocarriers to deliver antigen effectively, but also acted as an imaging agent for in vitro detection using confocal laser scanning microscopy (CLSM) and in vivo detection by MRI. **Figure 2**A–C illustrate the core–shell structure and magnetic properties of the $Fe_3O_4$@ZnO nanoparticles. Figure 2D compares the CLSM images of the nanoparticle-free dendritic cells and the dendritic cells loaded with $Fe_3O_4$@ZnO. It is clear that $Fe_3O_4$@ZnO nanoparticles emit green fluorescence under UV light irradiation, and the emission does not interfere with the blue fluorescence of the cell nuclei. The phagocytosis efficacy of $Fe_3O_4$@ZnO nanoparticles by the DCs was much higher than that of $Fe_3O_4$ nanoparticles, and more than 95% of DCs took up substantial amounts of $Fe_3O_4$@ZnO within 1 h of incubation. Since labeling DCs by conventional $Fe_3O_4$ nanoparticles required a long incubation period (typically ≈16–48 h), the ZnO shell was believed to facilitate the intracellular delivery of the nanoparticles.

Before the antigen delivery tests, the authors fused ZnO-binding peptide (ZBP) to a protein antigen (CEA). They found a triplicate tandem repeat of ZBP had a stronger binding affinity to ZnO, so they prepared the recombinant 3×ZBP–CEA fusion protein for incubation with the $Fe_3O_4$@ZnO nanoparticles. Two dyes, EEA1 and LAMP2, were used to label the endosomes and lysosomes, respectively, of the cells in advance. Figure 2E

shows that the 3×ZBP immobilized on the nanoparticles was efficiently delivered into the cytoplasm of DCs, and they formed peptide aggregates that partially co-localized with endosomes or lysosomes. When the $Fe_3O_4$@ZnO–3×ZBP–CEA complexes were incubated with the cells, the mean fluorescence intensity, representing the intracellular contents of CEA, increased 6 times over that of CEA alone, indicating that $Fe_3O_4$@ZnO–3×ZBP was able to deliver the CEA into DCs.

The MRI measurements were carried out on the mouse footpads in vivo. At 48 h after injection, the $Fe_3O_4$@ZnO-labeled DCs were identified at the localized hypointense regions in the lymph nodes (Figure 2F, left panel, red arrow), while the lymph nodes injected with ZnO-labeled DCs showed no reduction in the $T_2$ relaxation time (the image was not darkened; Figure 2F, left panel, yellow arrow). And in the control experiment of injecting $Fe_3O_4$@ZnO nanoparticles without DCs, $T_2$ reduction was also not detected (Figure 2F, right panel, green arrow). MRI results indicate that the $T_2$ reduction signals could only be induced by the $Fe_3O_4$@ZnO-labeled DCs. The immunohistochemistry of a draining lymph node injected with $Fe_3O_4$@ZnO-labeled DCs (Figure 2G) showed that the nanoparticles were mainly located at the T-cell zones and not at B-cell follicles. As a result, mice immunized with DCs labeled with $Fe_3O_4$@ZnO–3×ZBP–CEA showed enhanced tumor antigen specific T-cell responses, delayed tumor growth, and better survival than controls.[48]

The $Fe_3O_4$@ZnO–3×ZBP–CEA complex is a successful example of combining nanoprobe and nanocarrier together for cancer therapy in vivo, and the $Fe_3O_4$@ZnO core–shell structure perfectly allows both MRI and CLSM techniques for detection in vitro, but there are also shortcomings in these materials. As the authors mentioned, both $Fe_3O_4$@ZnO and $Fe_3O_4$@ZnO–3×ZBP nanoparticles aggregated heavily in the cells after phagocytosis, so they could not be degraded thoroughly by the endosomes or lysosomes. Moreover, photoluminescence spectra showed that the ZnO fluorescence on the $Fe_3O_4$ surface was rather weak, which impeded the fluorescent imaging of the material in vivo. To overcome these shortcomings, proper surface modification should be found to prevent particle aggregation both in cells and in blood, and the deposition of highly luminescent ZnO QDs onto the $Fe_3O_4$ surface would be better than coating the surface with a compact ZnO shell.

## 3. ZnO Nanoparticles for Drug Delivery

Drug-loaded nanostructured materials such as $Fe_3O_4$ nanoparticles, carbon nanotubes, mesoporous silica nanoparticles (MSNs) and polymer nanobeads, are able to enter cells through intracellular endocytic pathways and release drugs at target sites effectively,[49–55] especially when the drug itself cannot be taken up by cells.[56] In order to control the releasing process, different responding conditions have been employed; these include pH,[57] temperature,[58] and light.[59] Since pH values in tumors and inflammatory tissues are significantly lower than those in blood and normal tissues, pH-responsive drug delivery systems have outstanding advantages in their simple design and convenient operation. The pH-responsive systems usually employ pH-sensitive linkers[60] to connect hosts and guests, pH-responsive polymeric micelles[61] to encapsulate the drug, and pH-responsive molecules[62] to cover the pores of the MSNs. ZnO nanostructured materials, as a type of pH-responsive drug carrier, was suggested first in 2010,[63,64] and such materials have been developed rapidly in the past years.[65–68]

Zhu and Guo and co-workers[65] designed a novel drug delivery system to release doxorubicin (DOX) to HeLa cells in vitro. This system was composed of MSNs containing DOX inside the pores and ZnO QDs as lids covering the pores. ZnO QDs are stable around pH 7, but rapidly dissolve at pH < 6. ZnO itself is nontoxic, but after decomposition $Zn^{2+}$ ions are cytotoxic. Furthermore, the fluorescence of ZnO QDs can be used to monitor the drug delivery process. Therefore, the design of ZnO nanolids smartly utilized the features of ZnO QDs. Scanning electron microscopy (SEM) and TEM images show that ZnO nanoparticles covering the pores of MSNs can be cleared by incubation in pH 5.0 buffer solutions; the scheme of the system structure and the delivery mechanism are illustrated in **Figure 3**. In order to assemble such a system, carboxylic groups were anchored onto the outer surfaces of the MSNs first; then the inner channels of the MSNs were partially functionalized with amines, and the ZnO QDs were modified with aminopropyl groups. Since the DOX molecules were cationic and ZnO QDs had cationic surface groups, they were adsorbed by the anionic MSNs successively. These assembled composites were very stable in pH 7.4 buffer solutions, and almost no DOX leaked out of the MSNs. However, when the ZnO–MSN–DOX composites were dispersed into pH 5.0 buffer solutions, more than 30% of the adsorbed DOX were released from the channels within 5 h. Hence, in acidic compartments of the lysosomes (pH ≈ 4.5–5.0), ZnO nanolids were decomposed and the DOX molecules were released from the MSNs to kill the HeLa cells. It should be mentioned that although MSNs are stable for loading drugs and biocompatible during cell incubation, their degradation in the animal body is a controversial problem. Furthermore, their loading capacity and releasing effiency are not satisfying. In the above report by Zhu and Guo and co-workers, the DOX loading capacity was only 40 mg/g and the DOX releasing effiency was about 32% after 12 h of incubation in pH 5.0 buffer solutions. As a result, after DOX delivery, the remaining MSNs and the residual DOX in the MSNs would be problematic if such a system is applied in vivo. In a practical drug delivery system, the nanocarriers should be biodegradable or excretable, and they should have a considerable loading capacity for the drugs.

The latest work by our research group[68] suggested a new kind of ZnO@polymer–DOX system, which is biodegradable and possesses a high loading capacity of over 20 wt.%. Since the ZnO@polymer–DOX composite could be decomposed in acidic conditions, more than 90% of the DOX loaded onto the ZnO surface was released in pH 5.0 buffer solutions (**Figure 4**A). ZnO QDs were coated with biodegradable polymer shells, which exhibited low toxicity toward the human brain cancer cells U251. The toxicity of DOX-loaded ZnO nanoparticles should be lower than that of DOX itself theoretically, but actually, at appropriate concentrations the ZnO–DOX composites exhibited even higher cytotoxicity (Figure 4B). Such cytotoxicity enhancement effects by nanocarriers was ascribed to the improvement of drug internalization. Free DOX molecules

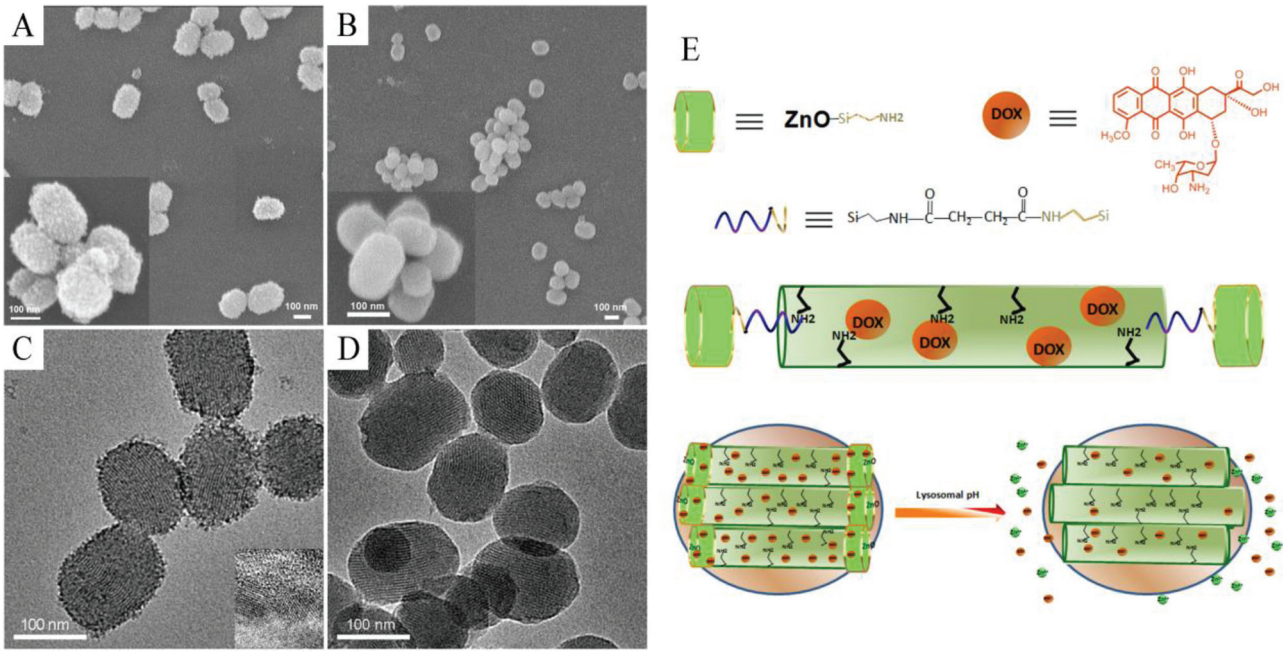


**Figure 3.** A) SEM and C) TEM images of MSNs capped by ZnO nanolids. The inset in C is a HRTEM image. B) SEM and D) TEM images of the sample obtained after incubation in pH 5.0 buffer solution, showing the dissolution of the ZnO nanoparticles. E) Schematic illustration of the structure of the DOX delivery system and the DOX release mechanism. Reproduced with permission.[65] Copyright 2011 American Chemical Society.

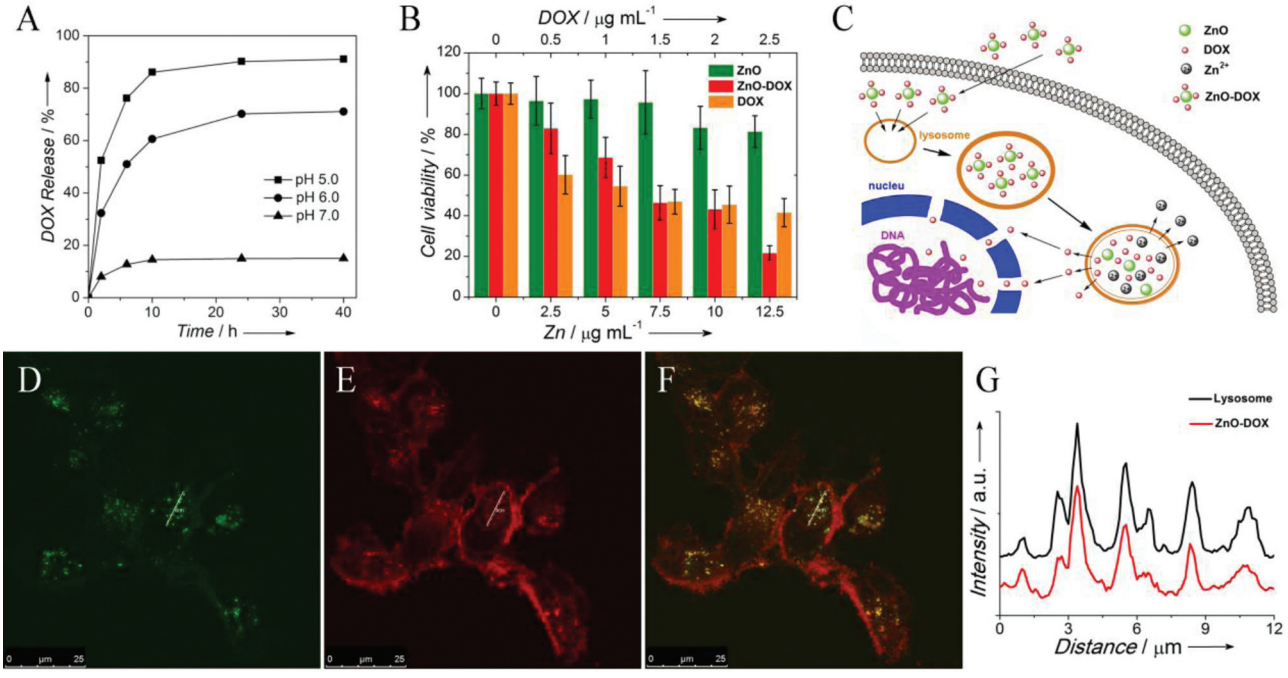


**Figure 4.** A) DOX release profile of ZnO@polymer–DOX at different pH values. B) Viability of U251 cells after treatment with ZnO@polymer QDs, ZnO@polymer–DOX composites, or free DOX for 48 h. The cytotoxicity of ZnO@polymer and ZnO@polymer–DOX were evaluated with regard to their Zn content (see the lower scale markings). The cytotoxicity of DOX and ZnO@polymer–DOX were evaluated with regard to their DOX content (see the upper scale markings). C) Schematic process of the DOX delivery from the ZnO@polymer–DOX composites in the cells. D–F) CLSM images of U251 cells after incubation with ZnO@polymer–DOX in the presence of lysotracker for 3 h. The green emission of D is from the lysotracker; the red emission of E is from ZnO@polymer–DOX, and F shows the merged picture of the above two channels. Scale bars = 25 μm. G) Fluorescence signal intensity of lysosomes (black) and ZnO@polymer–DOX (red) based on the white lines in images D and E, respectively. Reproduced with permission.[68]

penetrated cells through passive diffusion, and there would be a saturation concentration of DOX inside some cells with drug resistance, such as U251. When the DOX concentration outside cells increased continuously, the DOX cytotoxcity toward U251 reached a platform (about 40% of cell viability in Figure 4B). However, the situation changed when ZnO nanocarriers were employed. Once ZnO–DOX composites were taken up by cells, they would be engulfed by the endosomes and lysosomes, so the DOX saturation in the cellular fluid was not reached; that is, more and more ZnO–DOX would be taken up continuously. Finally, the ZnO–DOX composites decomposed in the lysosomes to release high concentrations of DOX molecules, thus exhibiting higher cytotoxcity. This mechanism is illustrated Figure 4C, and it was supported by detailed CLSM analyses as indicated in Figure 4D–G. After 3 h incubation, red fluorescence from DOX was found throughout the cytoplasm, and it was found to be especially localized in the lysosomes labeled by the green lysotracker (see the yellow points in Figure 4F). The fluorescence signals from Figure 4D and E match that of Figure 4G well, thus confirming that the ZnO@polymer–DOX nanoparticles were mainly decomposed in the lysosomes. Moreover, futher CLSM measurements proved that DOX molecules entered the nuclei to destroy DNA, and the $Zn^{2+}$ ions were also released from lysosomes and enriched by zincosomes in the cytoplasm.[68]

In fact, the dissolution behavior of ZnO nanoparticles at sequential nano–biological interfaces outside cells and the acidic environment of lysosomes have been studied in detail by Nel and co-workers.[69,70] They found that release of $Zn^{2+}$ ions in the cells could induce a series of harmful effects, such as lysosomal damage, mitochondrial perturbation and ROS production. As a result, ZnO nanoparticles without special modifications exhibited significant cytotoxicity. However, if ZnO nanoparticles are coated tightly with protective shells, they will be very stable in pH 7.4 buffer solutions and cell cultures, so that they will not dissolve outside cells. The drugs or biomolecules can be adsorbed on the ZnO surface or embedded in the shells around ZnO QDs, and they will be carried into cells safely by ZnO nanoparticles, where the drugs or biomolecules are released to perform their tasks.

## 4. Conclusion and Outlook

ZnO is listed as a safe substance by the United States Food and Drug Administration (21CFR182.8991), and it is stable towards air and sunlight in nature. ZnO nanoparticles, due to their outstanding advantages—nontoxicity towards animals and facile production using green chemical methods, have been commercialized in sunscreen creams and in ointments for treating skin disease. ZnO QDs, as reviewed in this paper, have exhibited promising applications in bioimaging and drug delivery, but their limitations remain an issue in recent researches.

With regard to bioimaging, the main drawback is the indispensable UV excitation for ZnO photoluminescence, which is determined by the bandgap of ZnO itself. UV light cannot penetrate the animal body like near infrared light, so recent research employing ZnO fluorescent probes are confined to CLSM investigations in vitro. Moreover, UV irradiation can damage cells and tissues, and arouse the interfering autofluorescence of biomolecules, affecting the accuracy of CLSM results. To overcome this difficulty, two strategies are suggested here. One is to adjust the ZnO bandgap by doping with other elements or forming complexes with other inorganic/organic compounds. The other is dependent on the breakthrough of two-photon/multi-photon microscopy techniques; that is, a red or near-infrared laser may excite ZnO, theoretically obtaining visible emission via an up-conversion mechanism. In addition, doping with rare-earth elements or coating with luminescent dyes could also resolve the excitation problem, but the final fluorescence would not be from ZnO itself. As an alternative to fluorescent imaging, MRI is also a good choice. Doping magnetic elements or incorporating magnetic complexes into ZnO QDs can produce binary fluorescence–magnetism probes, but the fluorescence quenching effects by the transition metals should be avoided by careful preparations. For example, a novel type of ferromagnetic materials, ZnO-based diluted magnetic semiconductor nanoparticles, could be incorporated with ZnO QDs to produce multifunctional probes.

With regard to drug delivery, the main challenge is obtaining ZnO-based nanocarriers that are stable in vivo. Since the bare ZnO nanoparticles are unstable in water and they can be dissolved in a weak acidic solution (pH < 6), surface modification is crucial for protecting ZnO nanoparticles in biological systems. According to previous reports, appropriate modification should contain two layers. One should be a hydrophobic layer tightly surrounding the ZnO nanoparticle isolating the ZnO core from water; the other should be an external hydrophilic layer making the entire particle dispersible in water. Furthermore, the preparation method for such core–shell structure is also crucial because ZnO nanoparticles are apt to aggregate, decompose, or lose fluorescence during chemical reactions. The stability requirement is not only concerning ZnO nanocarriers, but also the combination of ZnO and the drugs or biomolecules to be loaded. Theses guest molecules should not leak during blood circulation in vivo, so strong interactions with ZnO carriers is necessary, e.g., covalent bonds. With this in mind, ZnO hollow spheres or mesoporous ZnO nanoparticles may be the better carriers.

Finally, the toxicity of ZnO nanoparticles toward biological systems is a controversial issue. In general, many nontoxic substances become toxic when their sizes are reduced to the nanometer scale because the nanoscaled materials have very large surface-to-volume ratios and a large amount of unstable surface atoms which may render unexpected reactions with biomolecules. Although many cytotoxicity tests in vitro have indicated ZnO nanoparticles are able to release toxic $Zn^{2+}$ ions and produce destructive ROS, the in vivo animal injection tests have indicated that ZnO nanoparticles are almost entirely nontoxic. Therefore, ZnO nanoparticles themselves may be designed as anticancer or antibacterial agents for curing animals with diseases.

In a word, nanomaterials will have a bright future in biomedical applications, and ZnO nanoparticles are expected to make more exciting contributions in this field.

## Acknowledgements

This work was supported by the National Basic Research Program of China (2013CB934101), the National Natural Science Foundation of China (21271045), and the NCET-11-0115.

Received: April 18, 2013
Revised: June 4, 2013
Published online: June 21, 2013

[1] A. P. Alivisatos, *Science* **1996**, *271*, 933.
[2] X. Gao, Y. Cui, R. M. Levenson, L. W. K. Chung, S. Nie, *Nat. Biotechnol.* **2004**, *22*, 969.
[3] I. L. Medintz, H. T. Uyeda, E. R. Goldman, H. Mattoussi, *Nat. Mater.* **2005**, *4*, 435.
[4] R. A. Petros, J. M. DeSimone, *Nat. Rev. Drug Discovery* **2010**, *9*, 615.
[5] T. L. Doane, C. Burda, *Chem. Soc. Rev.* **2012**, *41*, 2885.
[6] M. Han, X. Gao, J. Z. Su, S. Nie, *Nat. Biotechnol.* **2001**, *19*, 631.
[7] T. Jamieson, R. Bakhshi, D. Petrova, R. Pocock, M. Imani, A. M. Seifalian, *Biomaterials* **2007**, *28*, 4717.
[8] J. L. Pelley, A. S. Daar, M. A. Saner, *Toxcicol. Sci.* **2009**, *112*, 276.
[9] N. Singh, B. Manshian, G. J. S. Jenkins, S. M. Griffiths, P. M. Williams, T. G. G. Maffeis, C. J. Wright, S. H. Doak, *Biomaterials* **2009**, *30*, 3891.
[10] M. Bruchez, M. Moronne, P. Gin, S. Weiss, A. P. Alivisatos, *Science* **1998**, *281*, 2013.
[11] M. De, P. S. Ghosh, V. M. Rotello, *Adv. Mater.* **2008**, *20*, 4225.
[12] A. M. Smith, H. Duan, A. M. Mohs, S. Nie, *Adv. Drug Deliver. Rev.* **2008**, *60*, 1226.
[13] A. M. Derfus, W. C. W. Chan, S. N. Bhatia, *Nano Lett.* **2004**, *4*, 11.
[14] S. J. Cho, D. Maysinger, M. Jain, B. Röder, S. Hackbarth, F. M. Winnik, *Langmuir* **2007**, *23*, 1974.
[15] U. Resch-Genger, M. Grabolle, S. Cavaliere-Jaricot, R. Nitschke, T. Nann, *Nat. Methods* **2008**, *5*, 763.
[16] J. H. Gao, K. Chen, R. G. Xie, J. Xie, S. Lee, Z. Cheng, X. G. Peng, X. Y. Chen, *Small* **2010**, *6*, 256.
[17] S. T. Yang, L. Cao, P. G. Luo, F. S. Lu, X. Wang, H. F. Wang, M. J. Meziani, Y. F. Liu, G. Qi, Y. P. Sun, *J. Am. Chem. Soc.* **2009**, *131*, 11308.
[18] Q. Liu, Y. Sun, T. Yang, W. Feng, C. Li, F. Li, *J. Am. Chem. Soc.* **2011**, *133*, 17122.
[19] X. Tang, E. S. G. Choo, L. Li, J. Ding, J. Xue, *Langmuir* **2009**, *25*, 5271.
[20] H. M. Xiong, *J. Mater. Chem.* **2010**, *20*, 4251.
[21] L. Spanhel, *J. Sol–Gel Sci. Technol.* **2006**, *39*, 7.
[22] L. Guo, S. Yang, C. Yang, P. Yu, J. Wang, W. Ge, G. K. L. Wong, *Chem. Mater.* **2000**, *12*, 2268.
[23] Y. S. Fu, X. W. Du, S. A. Kulinich, J. S. Qiu, W. J. Qin, R. Li, J. Sun, J. Liu, *J. Am. Chem. Soc.* **2007**, *129*, 16029.
[24] H. M. Xiong, Z. D. Wang, D. P. Liu, J. S. Chen, Y. G. Wang, Y. Y. Xia, *Adv. Funct. Mater.* **2005**, *15*, 1751.
[25] H. M. Xiong, Z. D. Wang, Y. Y. Xia, *Adv. Mater.* **2006**, *18*, 748.
[26] H. M. Xiong, D. P. Xie, X. Y. Guan, Y. J. Tan, Y. Y. Xia, *J. Mater. Chem.* **2007**, *17*, 2490.
[27] J. Han, H. Su, J. Xu, W. Song, Y. Gu, Y. Chen, W. J. Moon, D. Zhang, *J. Nanopart. Res.* **2012**, *14*, 726.
[28] H. M. Xiong, Y. Xu, Q. G. Ren, Y. Y. Xia, *J. Am. Chem. Soc.* **2008**, *130*, 7522.
[29] Z. Y. Pan, J. Liang, Z. Z. Zheng, H. H. Wang, H. M. Xiong, *Contrast Media Mol. Imaging* **2011**, *6*, 328.
[30] R. O. Moussodia, L. Balan, R. Schneider, *New J. Chem.* **2008**, *32*, 1388.
[31] X. S. Tang, E. S. G. Choo, L. Li, J. Ding, J. Xue, *Chem. Mater.* **2010**, *22*, 3383.
[32] R. O. Moussodia, L. Balan, C. Merlin, C. Mustind, R. Schneider, *J. Mater. Chem.* **2010**, *20*, 1147.
[33] H. Q. Shi, W. N. Li, L. W. Sun, Y. Liu, H. M. Xiao, S. Y. Fu, *Chem. Commun.* **2011**, *47*, 11921.
[34] H. J. Zhang, H. M. Xiong, Q. G. Ren, Y. Y. Xia, J. L. Kong, *J. Mater. Chem.* **2012**, *22*, 13159.
[35] H. M. Xiong, D. P. Liu, Y. Y. Xia, J. S. Chen, *Chem. Mater.* **2005**, *17*, 3062.
[36] H. M. Xiong, R. Z. Ma, S. F. Wang, Y. Y. Xia, *J. Mater. Chem.* **2011**, *21*, 3178.
[37] P. Lommens, F. Loncke, P. F. Smet, F. Callens, D. Poelman, H. Vrielinck, Z. Hens, *Chem. Mater.* **2007**, *19*, 5576.
[38] B. Panigrahy, M. Aslam, D. Bahadur, *J. Phys. Chem. C* **2010**, *114*, 11758.
[39] D. S. Bohle, C. J. Spina, *J. Phys. Chem. C* **2010**, *114*, 18139.
[40] I. Balti, A. Mezni, A. Dakhlaoui-Omrani, P. Léone, B. Viana, O. Brinza, L. S. Smiri, N. Jouini, *J. Phys. Chem. C* **2011**, *115*, 15758.
[41] D. Y. Inamdar, A K. Pathak, I. Dubenko, N. Ali, S. Mahamuni, *J. Phys. Chem. C* **2011**, *115*, 23671.
[42] S. Kumar, S. Chatterjee, K. K. Chattopadhyay, A. K. Ghosh, *J. Phys. Chem. C* **2012**, *116*, 16700.
[43] J. V. Foreman, J. Li, H. Peng, S. Choi, H. O. Everitt, J. Liu, *Nano Lett.* **2006**, *6*, 1126.
[44] H. M. Xiong, D. G. Shchukin, H. Möhwald, Y. Xu, Y. Y. Xia, *Angew. Chem. Int. Ed.* **2009**, *48*, 2727.
[45] Y. P. Du, Y. W. Zhang, L. D. Sun, C. H. Yan, *J. Phys. Chem. C* **2008**, *112*, 12234.
[46] L. W. Sun, H. Q. Shi, W. N. Li, H. M. Xiao, S. Y. Fu, X. Z. Cao, Z. X. Li, *J. Mater. Chem.* **2012**, *22*, 8221.
[47] Y. Liu, K. Ai, Q. Yuan, L. Lu, *Biomaterials* **2011**, *32*, 1185.
[48] N. H. Cho, T. C. Cheong, J. H. Min, J. H. Wu, S. J. Lee, D. Kim, J. S. Yang, S. Kim, Y. K. Kim, S. Y. Seong, *Nat. Nanotechnol.* **2011**, *6*, 675.
[49] L. Hu, Z. Mao, C. Gao, *J. Mater. Chem.* **2009**, *19*, 3108.
[50] J. J. Moon, B. Huang, D. J. Irvine, *Adv. Mater.* **2012**, *24*, 3724.
[51] M. J. Sailor, J. H. Park, *Adv. Mater.* **2012**, *24*, 3779.
[52] W. Fang, J. Yang, J. Gong, N. Zheng, *Adv. Funct. Mater.* **2012**, *22*, 842.
[53] X. J. Kang, Y. L. Dai, P. A. Ma, D. M. Yang, C. X. Li, Z. Y. Hou, Z. Y. Cheng, J. Lin, *Chem. Eur. J.* **2012**, *18*, 15676.
[54] J. Zhu, L. Liao, X. Bian, J. Kong, P. Yang, B. Liu, *Small* **2012**, *8*, 2715.
[55] D. Li, J. Tang, C. Wei, J. Guo, S. Wang, D. Chaudhary, C. Wang, *Small* **2012**, *8*, 2690.
[56] M. Wang, S. Yu, C. Wang, J. Kong, *ACS Nano* **2010**, *4*, 6483.
[57] J. Z. Du, X. J. Du, C. Q. Mao, J. Wang, *J. Am. Chem. Soc.* **2011**, *133*, 17560.
[58] J. Croissant, J. I. Zink, *J. Am. Chem. Soc.* **2012**, *134*, 7628.
[59] V. Voliani, F. Ricci, G. Signore, R. Nifosì, S. Luin, F. Beltram, *Small* **2011**, *7*, 3271.
[60] R. Liu, Y. Zhang, X. Zhao, A. Agarwal, L. J. Mueller, P. Y. Feng, *J. Am. Chem. Soc.* **2010**, *132*, 1500.
[61] X. B. Xiong, A. Lavasanifar, *ACS Nano* **2011**, *5*, 5202.
[62] Y. L. Zhao, Z. X. Li, S. Kabehie, Y. Y. Botros, J. F. Stoddart, J. I. Zink, *J. Am. Chem. Soc.* **2010**, *132*, 13016.
[63] K. C. Barick, S. Nigam, D. Bahadur, *J. Mater. Chem.* **2010**, *20*, 6446.
[64] Q. Yuan, S. Hein, R. D. K. Misra, *Acta Biomater.* **2010**, *6*, 2732.
[65] F. Muhammad, M. Y. Guo, W. X. Qi, F. X. Sun, A. F. Wang, Y. J. Guo, G. S. Zhu, *J. Am. Chem. Soc.* **2011**, *133*, 8778.
[66] F. Muhammad, M. Y. Guo, Y. J. Guo, W. X. Qi, F. Y. Qu, F. X. Sun, H. J. Zhao, G. S. Zhu, *J. Mater. Chem.* **2011**, *21*, 13406.
[67] Y. Liu, J. Yang, P. Zhang, C. Liu, W. Wang, W. Liu, *J. Mater. Chem.* **2012**, *22*, 512.
[68] Z. Y. Zhang, Y. D. Xu, Y. Y. Ma, L. L. Qiu, Y. Wang, J. L. Kong, H. M. Xiong, *Angew. Chem. Int. Ed.* **2013**, *52*, 4127.
[69] T. Xia, M. Kovochich, M. Liong, L. Mädler, B. Gilbert, H. B. Shi, J. I. Yeh, J. I. Zink, A. E. Nel, *ACS Nano* **2008**, *2*, 2121.
[70] A. E. Nel, L. Mädler, D. Velegol, T. Xia, E. M. V. Hoek, P. Somasundaran, F. Klaessig, V. Castranova, M. Thompson, *Nat. Mater.* **2009**, *8*, 543.